

Supporting Information

Activating MXene as a host of EMIm⁺ by electrochemistry-driven ferri-ion pre-intercalation

Wenjuan Han, Ming Lu, Haojie Li, Junnan Chen, Haibo Li, Bingsen Zhang,* Wei Zhang,*
Weitao Zheng*

1. Figures and Tables

Table S1. *d*-spacing values of ion pre-intercalated MXene by different methods.

MXenes	Intercalants	Methods	D (nm)	D'(nm)	Ref.
Ti ₃ C ₂ T _x	K ⁺	immersed in KOH solution	0.99	1.23	[1]
Ti ₃ C ₂ T _x	Li ⁺	LiCl	1.0	1.225	[2]
Ti ₃ C ₂ T _x	Li ⁺ &H ₂ O	immersed in LiCl solution	0.96	1.435	[3]
V ₂ CT _x	Na ⁺	immersed in NaOH solution	1.32	Lower	[4]
Ti ₃ C ₂ T _x	Na ⁺	immersed in NaOH solution	0.98	1.26	[5]
Ti ₃ C ₂ T _x	LiCl	electrochemical cycling	1.24	1.344	[6]
□	NaCl	□	□	1.313	
□	KCl	□	□	1.305	
Ti ₃ C ₂ T _x	Na ⁺	immersed in NaOH solution	0.981	1.24	[7]
Ti ₃ C ₂ T _x	Li ⁺	immersed in solution	No	1.52	[8]
□	Na ⁺	□	□	1.56	
□	K ⁺	□	□	1.4	
Ti ₃ C ₂ T _x	Li ⁺	immersed in LiOH solution	0.98	1.06	[9]
V ₂ CT _x	K ⁺	immersed in KOH solution	0.95	0.928	[10]

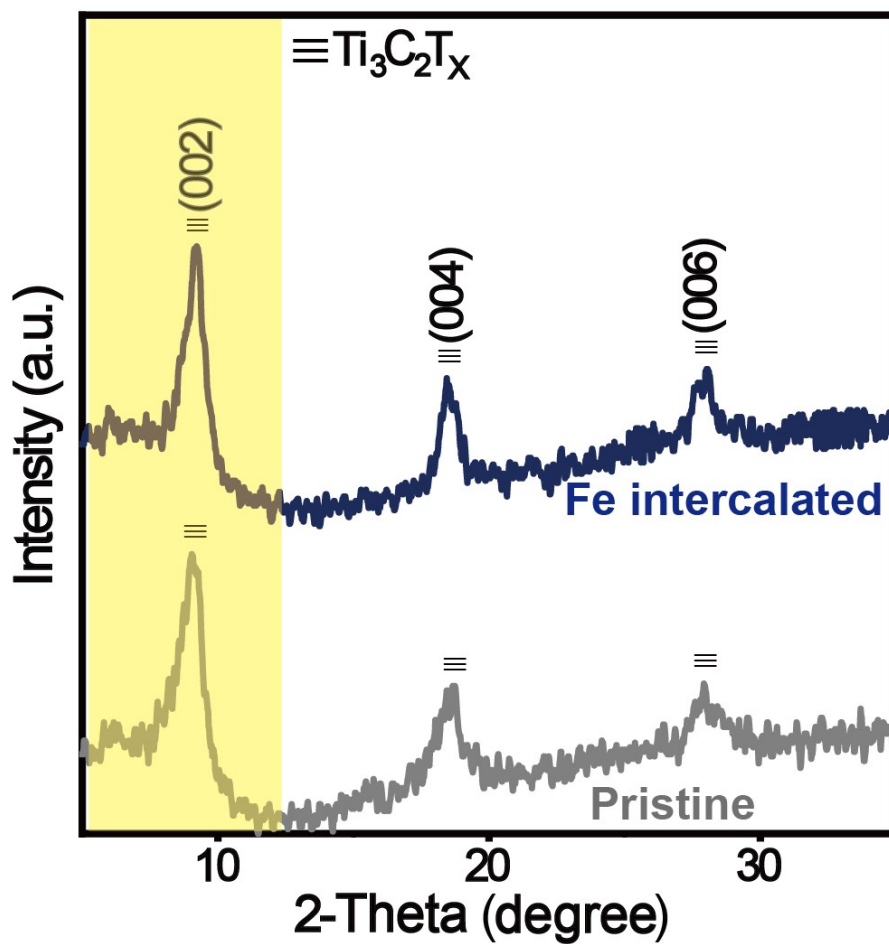


Figure S1. XRD patterns of pristine and Fe-intercalated ML Ti₃C₂T_x.

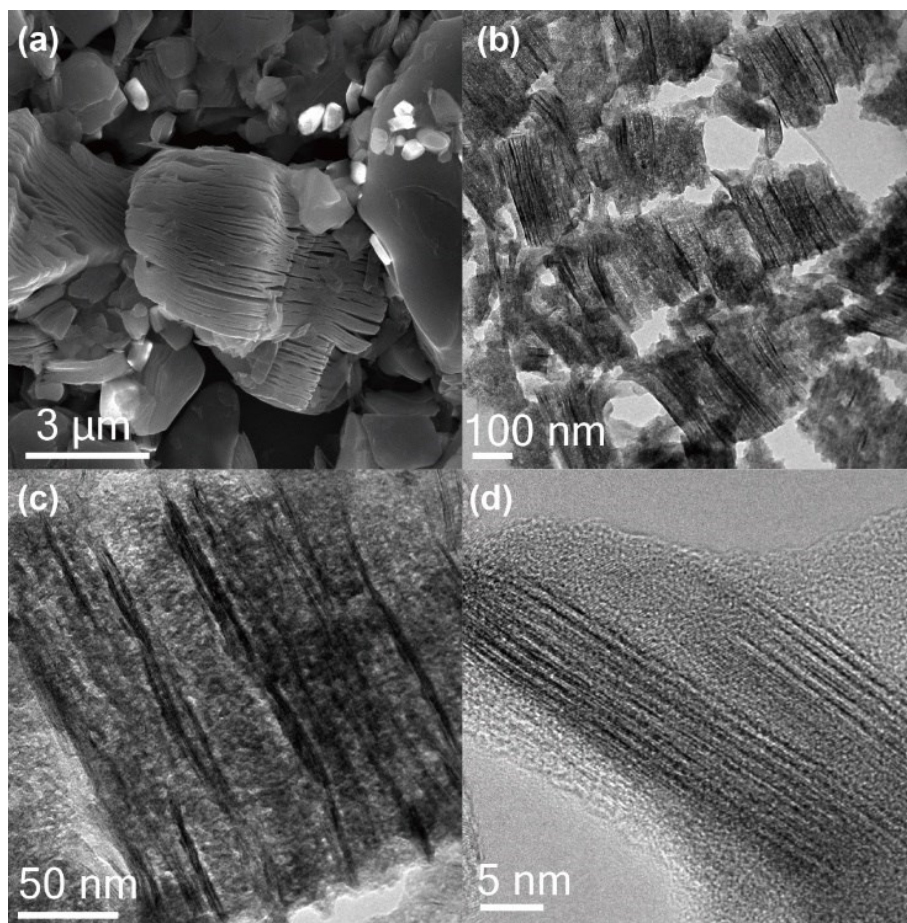


Figure S2. (a) SEM image and (b–d) TEM images of Fe-intercalated ML $Ti_3C_2T_x$.

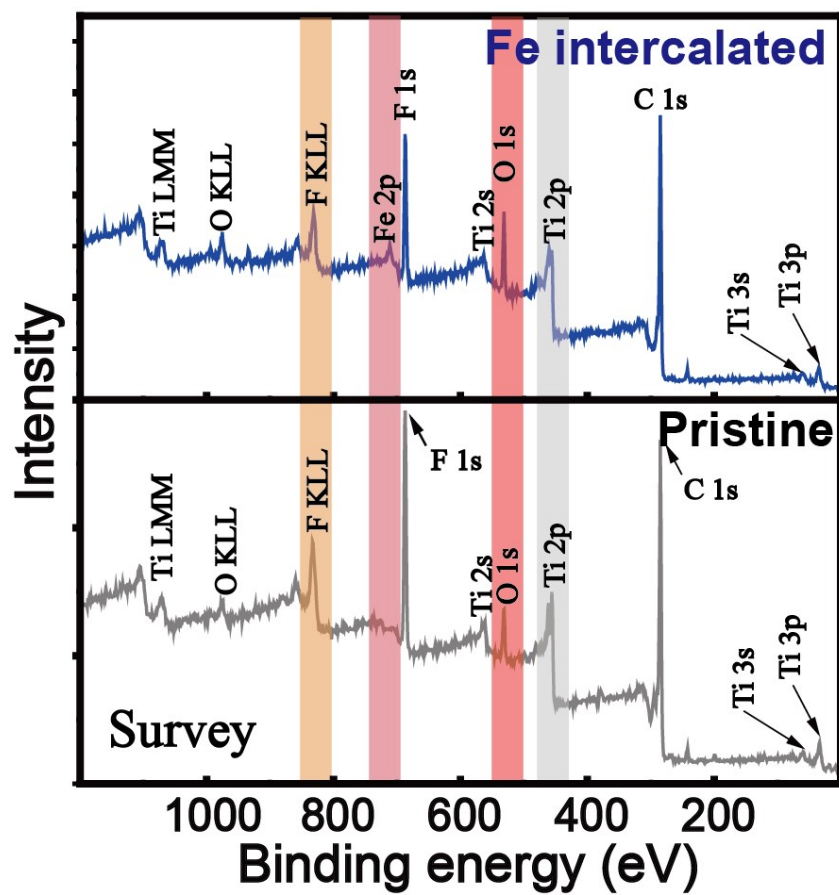


Figure S3. Survey of XPS spectra after 120 s of plasma sputtering.

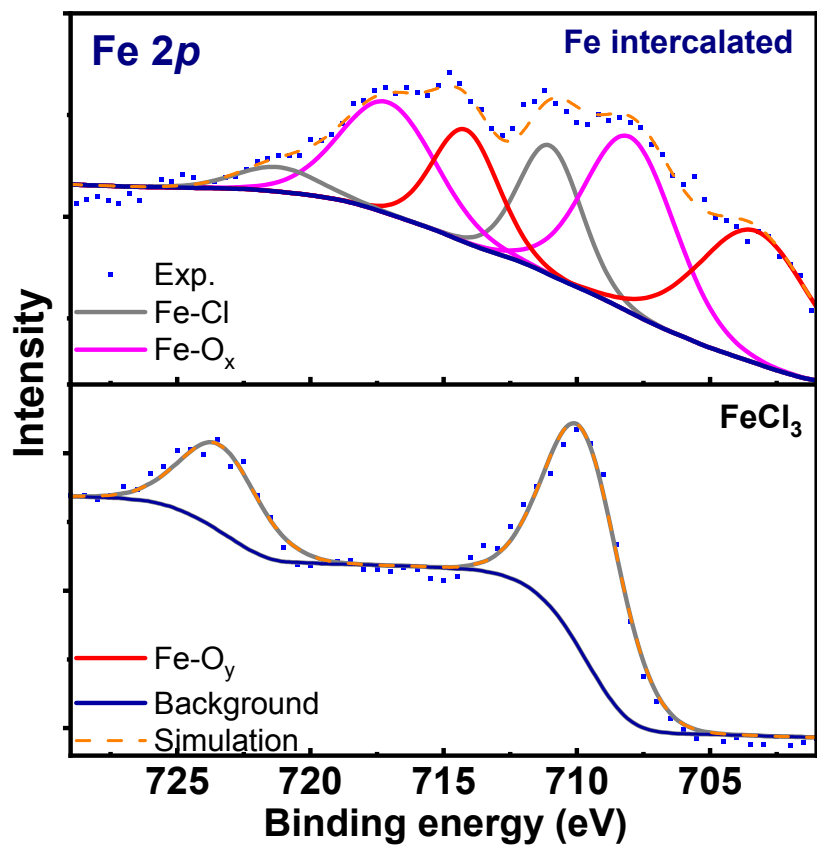


Figure S4. Fe 2p spectra in Fe-intercalated ML $\text{Ti}_3\text{C}_2\text{T}_x$ after 120 s of plasma sputtering.

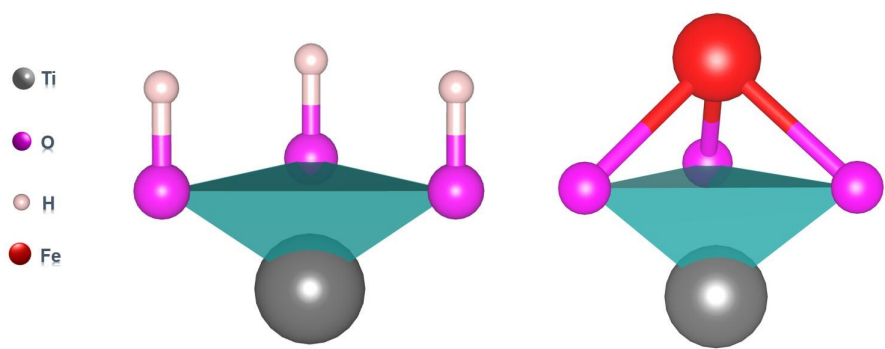


Figure S5. Side view of $\text{Ti}_3\text{C}_2\text{OH}$ and $\text{Ti}_3\text{C}_2\text{O-Fe(H)}$.

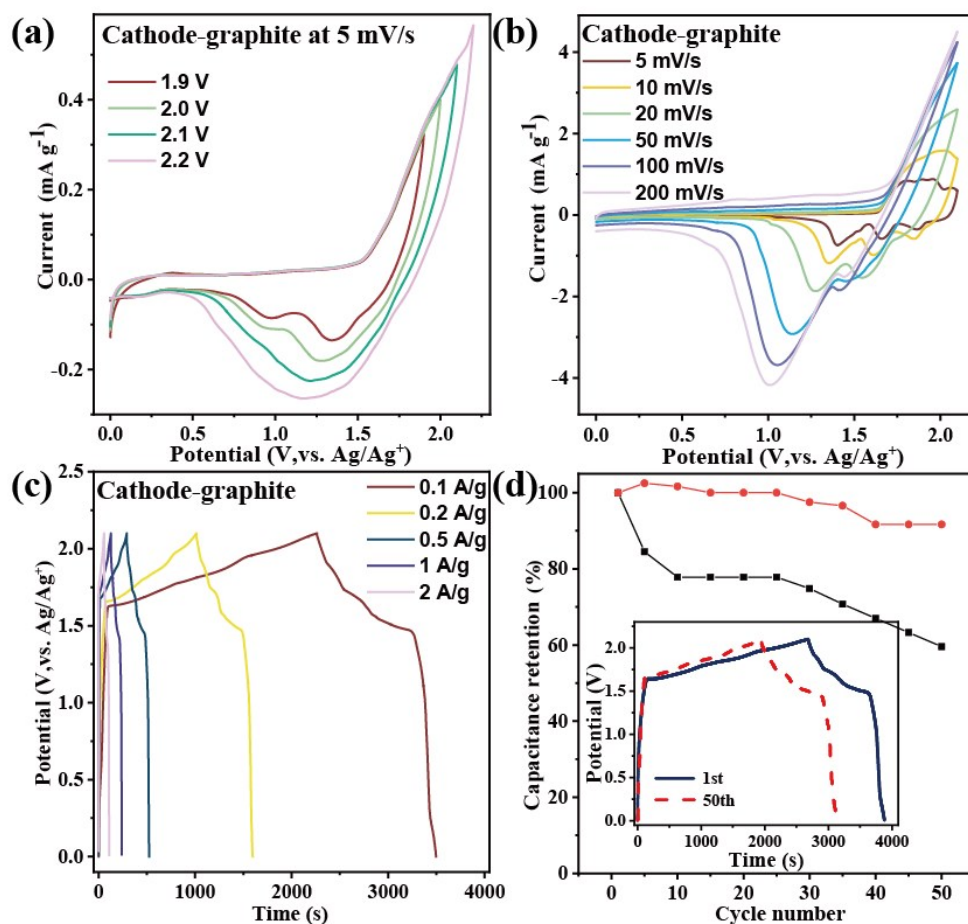


Figure S6. Electrochemical characterization of graphite cathodes: CV curves for different (a) potentials and (b) scan speeds, (c) GCD curves, and (d) cyclic stability.

Natural graphite is an excellent choice for the positive electrode material. The high insertion potential and fast kinetics of the anion intercalating into graphite enable the architecture of DIBs with both high energy and power density. $\text{EMIm}^+[\text{PF}_6]^-$ ionic liquid solvated in propylene carbonate/ethyl methyl carbonate was used as the electrolyte because of its low flammability, low volatility, high thermal stability, and broad electrochemical window. CV curves of the graphite cathode with different cut-off voltages are presented in Figure S6. To achieve improved capacitance and coulombic efficiency, the working voltage window was set to 0–2 V. In the CV curve with different scan speeds (Figure S6b) and galvanostatic charge–discharge (GCD) curves at the current density (Figure S6c), a broad peak appeared between 1.6 and 1.9 V during the oxidation process, which was attributed to the PF_6^- intercalation process.²⁷ In addition, during the reduction process, two broad peaks appeared between 1.8 and 0.5 V owing to the de-intercalation of anions from the graphite cathode is a stage process. GCD curves of the graphite cathode are presented in Figure S6d. The specific capacitance of the graphite cathode was calculated to be ~ 60 F/g, and the retention capacitance reached 92% (60% for the discharge process) after 50 cycles. The initial coulombic efficiency is 82.4%, and decreases to 65.3% upon the charge-discharge processes.

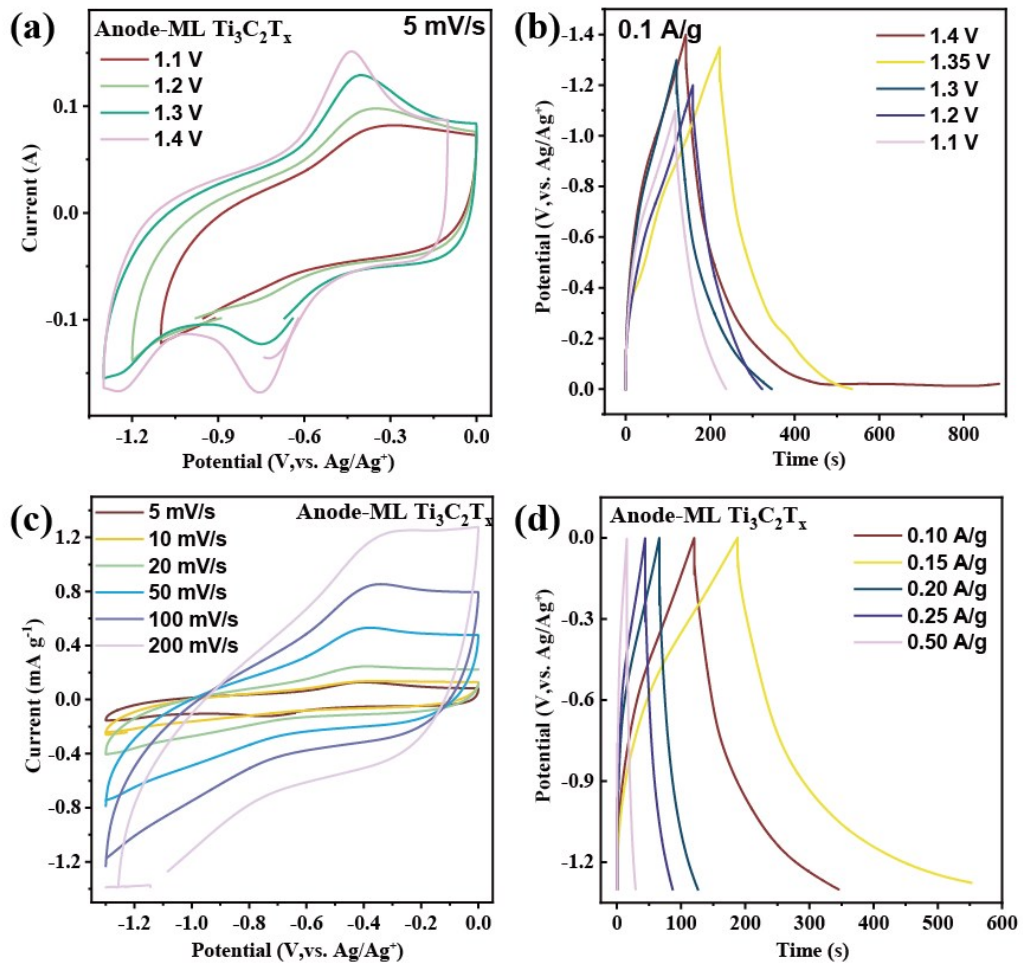


Figure S7. Electrochemical characterization of ML $\text{Ti}_3\text{C}_2\text{T}_x$ anodes. CV and GCD curves for different scan speeds and potential ranges.

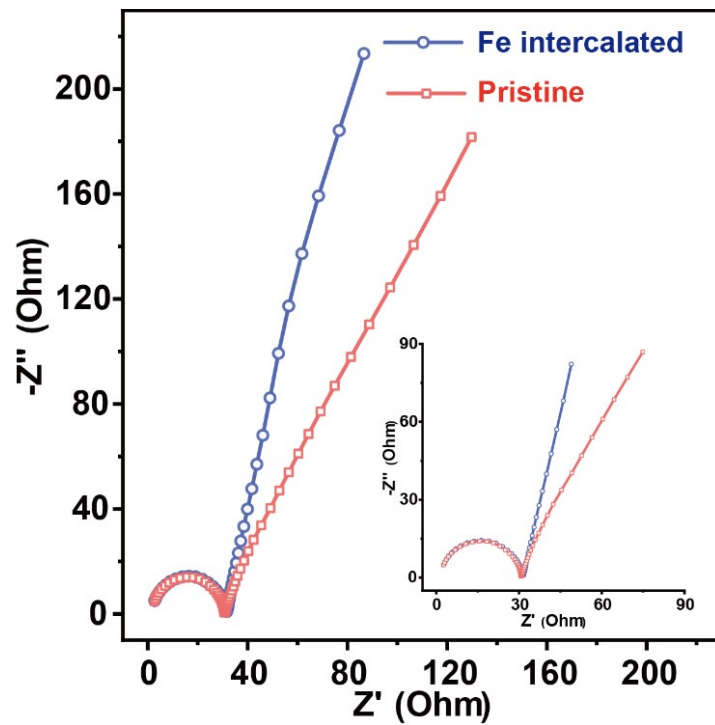


Figure S8. EIS curves of ML $\text{Ti}_3\text{C}_2\text{T}_x$ and Fe-intercalated ML $\text{Ti}_3\text{C}_2\text{T}_x$.

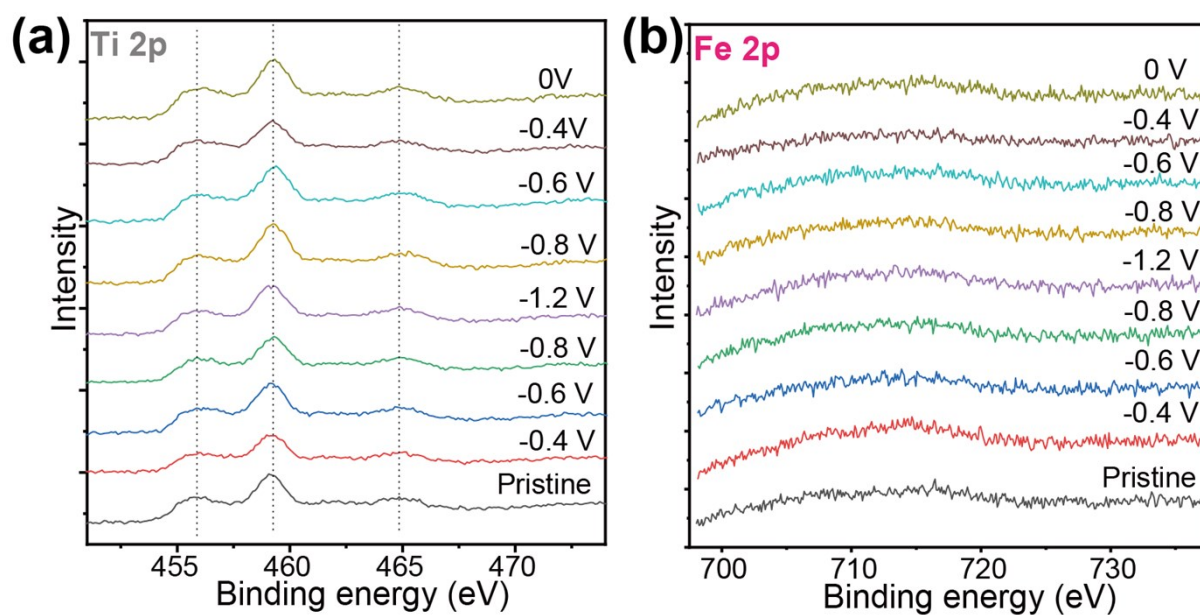


Figure S9. High-resolution XPS spectra of Ti 2p and Fe 2p.

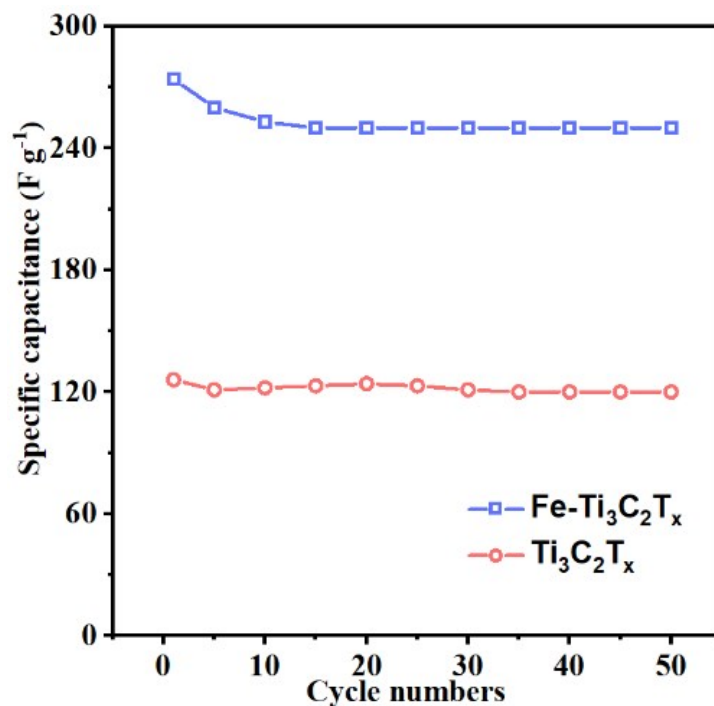


Figure S10. The discharge capacity of DIBs upon cycles.

References

- 1 N. C. Osti, M. Naguib, A. Ostadhossein, Y. Xie, P. R. C. Kent, B. Dyatkin, G. Rother, W. T. Heller, A. C. T. Van Duin, Y. Gogotsi and E. Mamontov, *ACS Appl. Mater. Interfaces*, 2016, **8**, 8859–8863.
- 2 M. Ghidui, J. Halim, S. Kota, D. Bish, Y. Gogotsi and M. W. Barsoum, *Chem. Mater.*, 2016, **28**, 3507–3514.
- 3 Q. Fu, J. Wen, N. Zhang, L. Wu, M. Zhang, S. Lin, H. Gao and X. Zhang, *RSC Adv.*, 2017, **7**, 11998–12005.
- 4 H. Zhang, L. Wang, C. Shen, G. Qin, Q. Hu and A. Zhou, *Electrochim. Acta*, 2017, **248**, 178–187.

- 5 J. Luo, C. Fang, C. Jin, H. Yuan, O. Sheng, R. Fang, W. Zhang, H. Huang, Y. Gan, Y. Xia, C. Liang, J. Zhang, W. Li and X. Tao, *J. Mater. Chem. A*, 2018, **6**, 7794–7806.
- 6 A. Qian, S. E. Hyeon, J. Y. Seo and C. H. Chung, *Electrochim. Acta*, 2018, **266**, 86–93.
- 7 H. Wang, J. Zhang, Y. Wu, H. Huang and Q. Jiang, *J. Phys. Chem. Solids*, 2018, **115**, 172–179.
- 8 D. Zhao, M. Clites, G. Ying, S. Kota, J. Wang, V. Natu, X. Wang, E. Pomerantseva, M. Cao and M. W. Barsoum, *Chem. Commun.*, 2018, **54**, 4533–4536.
- 9 C. Xue, Y. He, Y. Liu, P. Saha and Q. Cheng, *Ionics*, 2019, **25**, 3069–3077.
- 10 F. Ming, H. Liang, W. Zhang, J. Ming, Y. Lei, A. H. Emwas and H. N. Alshareef, *Nano Energy*, 2019, **62**, 853–860.